Assessing the performance of windowed H-1 CRAMPS methods, on biological solids, at high-field and MAS up to 35 kHz

4 AUTHORS:

Luís Mafra
University of Aveiro
86 PUBLICATIONS **1,254** CITATIONS

SEE PROFILE

Cristina Coelho
Pierre and Marie Curie University - Paris 6
34 PUBLICATIONS **863** CITATIONS

SEE PROFILE

Renée Siegel
University of Bayreuth
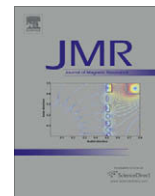**36** PUBLICATIONS **651** CITATIONS

SEE PROFILE

Joao Rocha
University of Aveiro
455 PUBLICATIONS **9,801** CITATIONS

SEE PROFILE

Assessing the performance of windowed ^{1}H CRAMPS methods, on biological solids, at high-field and MAS up to 35 kHz

Luís Mafra *, Cristina Coelho, Renée Siegel, João Rocha

Department of Chemistry, CICECO, University of Aveiro, Campus de Santiago, 3810-193 Aveiro, Portugal

ABSTRACT

The performance of various high-resolution 1D ^{1}H CRAMPS pulse schemes at moderate and high static magnetic fields (400 MHz and 800 ^{1}H Larmor frequencies) and spinning rates up to 35 kHz, using state-of-the-art electronics is compared. The performance of the ^{1}H windowed acquisition decoupling schemes, wDUMBO, wPMLG3 and wSAM3 is investigated using their effective *z*-rotation variants on glycine and other small biological molecules, tripeptide reduced glutathione and nucleoside uridine. ^{1}H CRAMPS spectra, recorded with windowed ^{1}H–^{1}H decoupling methods and fast MAS (35 kHz) and high-field are reported for the first time. ^{1}H spectra exhibiting outstanding resolution and completely free from any artifact are also shown. The effect on spectra quality of the decoupling *rf* cycle and rotor periods ratio (τ_C/τ_R) and the power requirements needed for each windowed ^{1}H CRAMPS methods are discussed.

© 2008 Elsevier Inc. All rights reserved.

1. Introduction

Due to its high sensitivity and high natural abundance, ^{1}H NMR spectroscopy is routinely used for the characterization of structure and dynamics in solution state NMR. This is not so for solids because of the dominant strong homonuclear ^{1}H–^{1}H dipolar couplings, which broaden the proton resonances to typically a few tens of kHz for rigid networks.

For rigid non-deuterated solids, fast magic-angle spinning (MAS) and periodic multiple *rf* pulses [1,2], may be employed to partially remove the dipole–dipole interactions. Simple rotation of the sample at the magic-angle is not sufficient to fully average out ^{1}H dipolar couplings, even at the highest rates available today (up to 70 kHz). Periodic multiple-pulse decoupling sequences average out the homonuclear dipolar interactions in spin-space but do not remove the line broadening due to chemical shift anisotropy. High-resolution ^{1}H spectra in solid-state NMR may be attained using Combined Rotation And Multiple-Pulse Spectroscopy (CRAMPS) [3], which consists in combining spin-space and real-space averaging.

Several ^{1}H CRAMPS techniques, based on a quasi-static regime, are available using windowless [4–18] and windowed [18–23] pulse sequences. So far, the application of these sequences has been limited to slow and moderate spinning rates. For example, ^{1}H CRAMPS methods such as Frequency Switched Lee–Goldburg (FSLG), Phase Modulated Lee–Goldburg (PMLG) and Decoupling Under Mind Boggling Optimisation (DUMBO) have been increasingly used on their windowless forms, with the later performing well up to 24 kHz [15]. The windowed versions of these pulse sequences have only been tested up to 16 kHz and comprehensive reports are scanty on the investigation of their dependence on various experimental parameters, particularly very-fast MAS rate. Rotor-synchronised symmetry-based sequences [24–26] have also been used in the design of windowless ^{1}H CRAMPS schemes. The $R10_2^5$ symmetry-based sequence performs well at 30 kHz MAS while calculations indicate that the sequence $R16_5^8$ may perform well at 60 kHz, employing relatively low *rf* power requirements (ν_1 = 144 kHz) [26]. Moreover, similar RN_n^ν Smooth Amplitude-Modulated (SAM) symmetry-adapted pulse sequences, have been recently suggested to decouple ^{1}H spins at MAS rates up to 65 kHz (windowless) and 30 kHz (windowed variants) [27–29]. SAM consists of applying a cosine-modulated shape, instead of a square, pulse.

Recently, we have assessed the performance of several Lee–Goldburg based ^{1}H CRAMPS techniques [30] and their dependence on several experimental parameters. Following up this work, here, we wish to compare the performance of wPMLG3, wDUMBO and wSAM3 at fast MAS rates (up to 35 kHz), using

two different magnetic fields (9.4 and 18.8 T) and a fast electronics NMR console.

This study is carried out using glycine and the small biological molecules, uridine and reduce tripeptide glutathione (GSH). To the best of our knowledge no papers are available on windowed ^{1}H CRAMPS at fast MAS rates and high magnetic fields.

2. Experimental

^{1}H NMR spectra were recorded on 9.4 T Bruker DSX 400 WB and 18.8 T Bruker Avance-III 800 NB spectrometers using 2.5, 3.2 and 4 mm double resonance probes.

^{1}H CRAMPS Experiments were performed on glycine (Aldrich), uridine (Aldrich) and GSH (Merck) samples and spinning at the magic-angle in ZrO_2 rotors (samples not restricted to the center of the rotor). The experimental scaling factors (λ_{exp}) of ^{1}H CRAMPS spectra were determined by comparison with a ^{1}H glycine spectra recorded using a single-pulse experiment (SPE) and MAS at 20 kHz. λ_{exp} is calculated from $\Delta\delta^{scaled}$ between the NH_3^+ and CH_3 peaks of a scaled ^{1}H CRAMPS spectrum, and $\Delta\delta^{SPE}$ of a ^{1}H SPE spectrum [$\lambda_{exp} = \frac{\Delta\delta^{scaled}}{\Delta\delta^{SPE}}$]. Chemical shifts are quoted in parts per million (ppm) from tetramethylsilane (TMS). The sample temperature during the various ^{1}H CRAMPS spectra recorded at the different spinning rates was kept constant at 298 K using a temperature controlling unit.

All the different windowed ^{1}H acquisition schemes were recorded using:

- A detection window (t_W) of 7 μs (Bruker DSX) and 5.6 μs (Bruker Avance III);
- A transmitter blanking of 0.7 μs;
- A fast digital receiver unit able to sample one complex data point by averaging 32 points sampled at 20 MHz over 1.6 μs (Bruker Avance III only);
- A dwell time calibrated according to the rf cycle period plus t_W of each CRAMPS sequence.

Further experimental details used to obtain the different ^{1}H spectra may be found in the figure captions.

3. Results and discussion

3.1. Investigating windowed ^{1}H CRAMPS methods on glycine

3.1.1. General considerations

The three windowed CRAMPS techniques, wPMLG3, wDUMBO and wSAM3 (Fig. 1) were all used employing exactly the same pulse sequence. In practice, using the same pulse sequence it is just necessary to change the respective decoupling shape. Thus, excluding the shape calibration, i.e., the parameters pertinent to each decoupling method, all the other parameters (mostly depending on the hardware such as the dead time, t_W, transmitter blanking, etc.) were the same. We have applied the recently developed improvement made on wPMLGn decoupling, the z-rotation variant [20,31], which consists of a supercycle of two consecutive PMLGn shape pulses having a 180° phase switch between each other. The same principle was also applied to wDUMBO. The use of an effective z-rotation has been shown to be less sensitive to rf imperfections over a broad range of ^{1}H offsets and also to remove/reduce image peaks as well as the zero line frequency. The z-rotation versions of wPMLG3 or wDUMBO may also be noted wPMLG3^{XX} and wDUMBO^{XX} (Fig. 1), respectively. However, for the sake of simplicity, we drop this notation for both sequences and from now on, wPMLG3 and wDUMBO refer to their z-rotation variants. The wSAM3 method is a symmetry-adapted sequence ($R6_1^3$). We now examine the three different techniques, studying their sensitivity to several experimental parameters (shape pulse length, rf field strength, spinning frequency, and B_0 field).

3.1.2. Calibrating the rf cycle lengths and field strengths of windowed ^{1}H CRAMPS

The wPMLG3 scheme consists of 6 sequential pulses with phases ϕ_i with i = 1–6 (Fig. 1a). The phase increment, $\Delta\phi_i$ is 207.8/3 beginning with $\Delta\phi_i/2$. The rf phase of the second half of the wPMLG3 sequence [i = 4–6] is reversed by 180° with respect the first half [i = 1–3]. The PMLG3 shape was preferred to the more used PMLG5, because of its enhanced ^{1}H resolution (Fig. S1). In addition, at faster spinning rates, a shorter CRAMPS cycle period (τ_C) is needed, thus making PMLG3 more adequate than PMLG5 for a given rf field strength. The optimization of wPMLG3 is quite
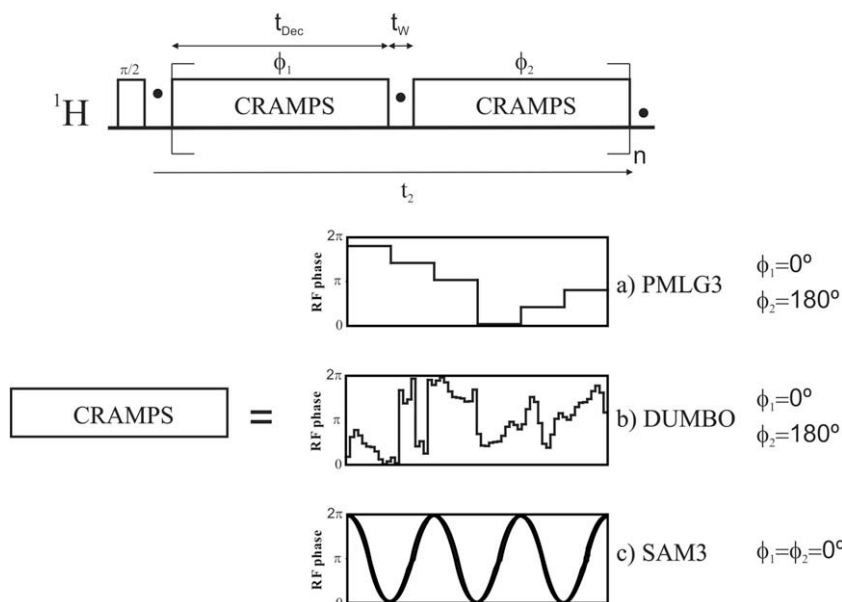

Fig. 1. Windowed ^{1}H CRAMPS pulse sequence employing the (a) PMLG3, (b) DUMBO and (c) SAM3 decoupling schemes.

straightforward: aside the ^{1}H rf offset frequency, one just needs to find the rf field strength necessary to obtain the correct PMLG3 pulse length which is previously estimated according to the Lee–Goldburg condition [30], or vice-versa. However, the choice of the optimum CRAMPS cycle period (τ_C with $\tau_C = t_{Dec} + t_W$) should be carefully checked in order to avoid certain unwanted conditions [13]. This will be discussed later on the wDUMBO technique. Maintaining constant the rf pulse length while changing the rf field strength of the decoupling sequence (data not shown), we observe that wPMLG3 is not excessively sensitive to the variation of the latter (for a given spinning rate), affording good ^{1}H resolution over a wide range of Decibel, making wPMLG3 a rather robust decoupling technique.

The wDUMBO shape also consists of a phase-modulated function. We have employed a shape composed by one cycle of 64 steps (Fig. 1b) built from the combination of six complex Fourier coefficients [15]. Like wPMLG3, we just need to calibrate the rf pulse length and the rf field strength, accordingly. For a given pulse length, the ^{1}H resolution is maximal over a narrower Decibel region, in comparison to wPMLG3 (data not shown). The pulse length for the DUMBO shape is usually set to 32 μs [15,17] for a 100 kHz decoupling strength using a spinning rate of 12.5 kHz. We now show the influence of several experimental parameters on the resolution of ^{1}H spectra.

Fig. 2 illustrates the optimization curves, using wDUMBO, showing the decoupling rf pulse length (t_{Dec}) variation for different spinning rates and rf field strengths. t_{Dec} is a key parameter

to achieve good ^{1}H resolution. We observe maxima and minima intensities, when employing different t_{Dec} values, which do not depend on the rf field strength [compare Fig. 2(II and III) or Fig. 2(V and VI)] albeit depending on the rotor and CRAMPS cycle periods i.e., the ratio τ_R/τ_C. Lesage et al. reported a similar behavior although keeping t_{Dec} and the nutation frequency at a constant value, respectively, while varying the spinning rate [15]. It is known that these minima are attributed to destructive interferences between the rotor period and the homonuclear decoupling cycle modulations, which occur for certain values of τ_R/τ_C [13,32,33]. Vinogradov et al. have used a bimodal Floquet analysis to calculate the exact position of these minima occurring for certain Floquet crossing levels, i.e., when $\kappa\tau_R + \nu\tau_C = 0$ and when $|\nu| < 5$ or $\tau_R/\tau_C < 5$, with κ and ν being integer numbers [13].

Having set the ^{1}H rf offset frequency approximately in the center of the ^{1}H resonances and selected an appropriate spectral width, Fig. 2 illustrates what has to be done to fully optimize a given windowed ^{1}H decoupling sequence. This figure shows, for wDUMBO, how the ^{1}H resolution is affected by varying the τ_C (or t_{Dec}), τ_R and ν_1. Most observed minima may be assigned using the Floquet analysis. It may be seen that the deepest minimum conditions occur when $\tau_C/\tau_R = 0.25$ and 0.5, which correspond to $\{\nu, \kappa\}$ values of $\{4, -1\}$ ('a' conditions in Fig. 2, Table 1) and $\{2, -1\}$ and/or $\{4, -2\}$ ('c' conditions in Fig. 2, Table 1), respectively. A few of these minima could not be assigned using this rationale, however they may be attributed to other types of crossing levels, which may occur, for example, when the scaled chemical shift values of the protons are taken into account [13].

By keeping a constant spinning rate, the maximum region depends on the rf field strength (Fig. 2V and VI). A shorter pulse length gives a better resolution with a larger rf field strength. Fig. 2 further shows that as the spinning rate increases the minima corresponding to each different crossing level change their positions and become closer to each other. Above a certain spinning rate, for instance 20 kHz (Fig. 2V and VI), two maxima are observed near the Floquet crossing levels 'b' and 'd' (Fig. 2V and VI, Table 1) when varying τ_C, 5 μs < τ_C < 40 μs. Employing ν_R = 20 kHz, the best ^{1}H resolution using ν_1 = 150 kHz (Fig. 2V) is obtained with t_{Dec} = 12.5 μs or $\tau_C \cong 18.5$ (corresponding to $\tau_R/\tau_C \cong 2.7$), while at ν_1 = 100 kHz, a longer pulse length of t_{Dec} = 27 μs (corresponding to $\tau_R/\tau_C \cong 1.5$) is needed for wDUMBO, which is equivalent to a $\tau_C = t_{Dec} + t_W \cong 33$ μs. In contrast, at MAS rates of 35 kHz best resolution/intensity is reached at $\tau_R/\tau_C \cong 1.45$ employing a rf field strength of 150 kHz. For DUMBO decoupling, a very thorough optimization of t_{Dec} and rf field strength are mandatory in order to obtain the best ^{1}H resolution. The same should be valid for the remaining ^{1}H CRAMPS techniques. This is even more important at high spinning rates because τ_R is shorter and the crossing levels
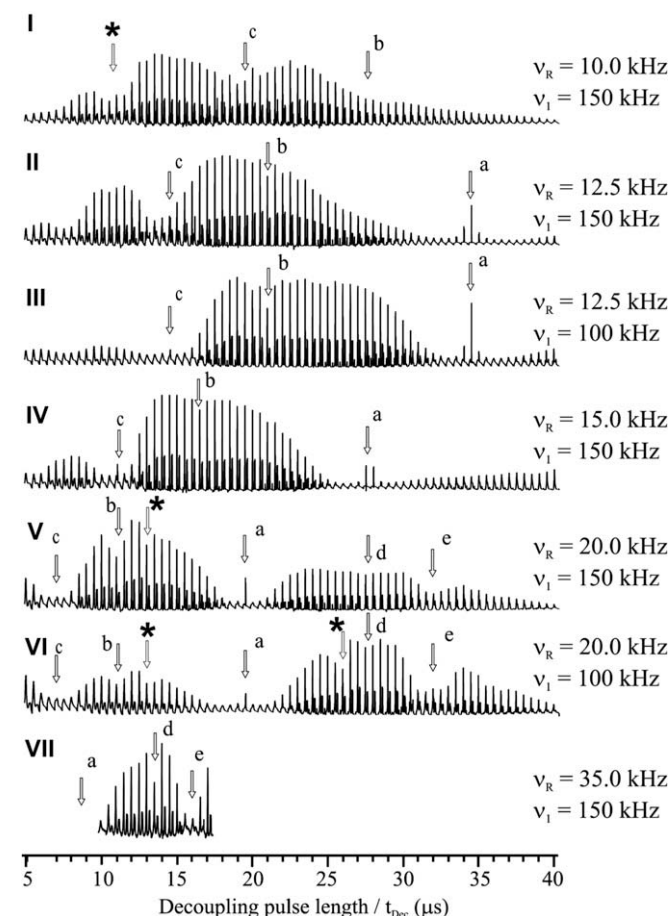

Fig. 2. Signal intensity/resolution variation as a function of the wDUMBO rf pulse length (t_{Dec}) at different spinning rates and rf field strengths. Minima positions corresponding to different Floquet crossing levels are depicted by letters 'a–e' (Table 1). Asterisks depict unassigned minima.

Table 1
List of τ_C (μs) values calculated for the different Floquet crossing levels at different spinning frequencies (see Fig. 2 for the visualization of the conditions 'a–e').

$\{\nu, \kappa\}$	ν_R (kHz)				
	10.0	12.5	15.0	20.0	35.0
$\{1,-1\}$	100	80.0	66.7	50.0	28.6
$\{2,-1\}$a	50.0	40.0	33.3	25.0	14.3
$\{3,-1\}$b	33.3	26.7	22.2	16.7	9.52
$\{4,-1\}$c	25.0	20.0	16.7	12.5	7.14
$\{1,-2\}$	200	160.	133.3	100.	57.3
$\{2,-2\}$	100	80.0	66.7	50.0	28.6
$\{3,-2\}$d	66.7	53.3	44.4	33.3	19.0
$\{4,-2\}$a	50.0	40.0	33.3	25.0	14.3
$\{3,-3\}$	100	80.0	66.7	50.0	28.6
$\{4,-3\}$e	75.0	60.0	50.0	37.5	21.5

corresponding to precise values of τ_R/τ_C will be more sensitive to any pulse variation, due to their close proximity (Fig. 2VII). For instance, at MAS rates of 35 kHz.

The SAM3 shape (Fig. 1c) consists of three periods of a cosine function spanning one rotor period. Although symmetry-based sequences are rotor synchronized, windowed SAM3 should not be rotor synchronized due to the addition of t_W for data point sampling (i.e., $\tau_C = t_{Dec} + t_W \neq \tau_R$) [27]. It has been shown that since homonuclear dipolar interaction is active during t_W, it is important that the windows are placed at different periods of the rotor modulation so that related dephasings occurring at successive windows compensate each other [34]. In this way the selection rules may still be valid for wSAM3. In general, SAM3 only requires the optimization of the rf field strength.

3.1.3. Comparing the different windowed ^1H CRAMPS techniques on glycine

These three different techniques (Fig. 3) are now compared. As expected, for simple ^1H SPE spectra, faster spinning rates and a higher B_0 field improves the spectral resolution. Nevertheless, the spectral resolution is still modest and, thus, CRAMPS decoupling methods should be used [18]. No considerable resolution improvement was observed in the ^1H wPMLG3 spectra of glycine recorded at high B_0 fields (Fig. 3g and i) and fast spinning rates (Fig. 3e and f or Fig. 3g and h). At $\nu_R = 15$ kHz, the wDUMBO ^1H spectrum is slightly better resolved than the spectrum of wPMLG3 (Fig. 3e and g). Although wPMLG3 and wDUMBO are quasi-static derived methods, they are still performing well at fast spinning rates (at least up to 35 kHz, Fig. 3f and h). There is no resolution loss at fas-
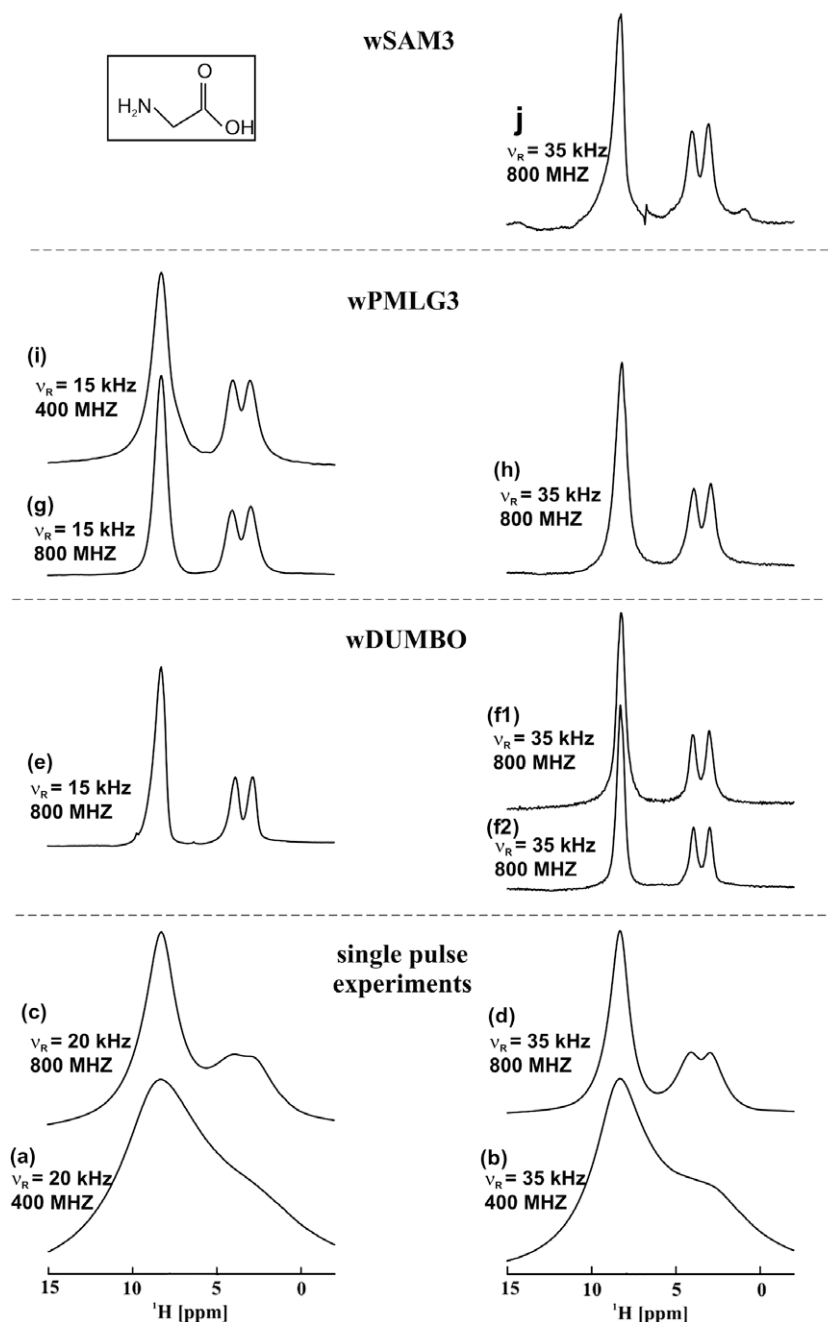

Fig. 3. ^1H glycine spectra recorded employing: (a–d) ^1H SPE; wDUMBO decoupling using (e) $\nu_1 = 112$ kHz, (f1) $\nu_1 = 195$ kHz and (f2) $\nu_1 = 146$ kHz; wPMLG3 decoupling using (g) $\nu_1 = 112$ kHz, (h) $\nu_1 = 146$ kHz and (i) $\nu_1 = 70$ kHz; wSAM3 decoupling using (j) $\nu_1 = 110$ kHz. Recycle delay: 3 s.

ter MAS rates. In fact, the ^{1}H spectra are slightly better resolved at 35 than 15 kHz on GSH (Fig. 5e and f). Comparing the techniques, clearly wDUMBO performs slightly better than wPMLG3 and wSAM3. The latter two yield spectra of similar resolution (Fig. 3h and j). It is worth noting that the implementation of an effective z-rotation method, affords wPMLG3 and wDUMBO ^{1}H spectra devoid of the central axial artifact, which is, however, observed in the wSAM3 spectrum (the same rf offset was used in all sequences). Moreover, the wSAM3 spectrum is noisier with some baseline distortions. Nevertheless, wSAM3 is less stringent on rf field power. For example, using $\nu_R = 35$ kHz, wSAM3 requires 25% less rf field strength ($\nu_1 = 110$ kHz) than wDUMBO and wPMLG3 ($\nu_1 = 146$ kHz). We recorded wDUMBO ^{1}H spectra using rf field strengths of 146 (Fig. 3f2) and 195 kHz (Fig. 3f1) but no additional line narrowing was observed. Presumably, faster spinning would

be required in order to improve the ^{1}H spectra resolution at the stronger rf field employed in this work ($\nu_1 = 195$ kHz). The symmetric (i.e., symmetric with respect to the carrier frequency) rf-rotor frequency lines [20] appearing on some wDUMBO and wPMLG3 ^{1}H spectra (not shown in the figures) were always located outside the region of ^{1}H signals over all range of spinning rates tested (up to 35 kHz). Thus, setting the carrier ^{1}H frequency at the center of the ^{1}H signals no problems were obtained due to the superposition of rf-rotor frequency lines and ^{1}H signals.

Glycine is a good initial test sample to optimize the various experimental parameters. However, more complex compounds, having ^{1}H nuclei in distinct functional groups, may provide a better assessment of the robustness of each decoupling method. In the following section, we will restrict our study to wPMLG3 and wDUMBO, which seem to outperform wSAM3.
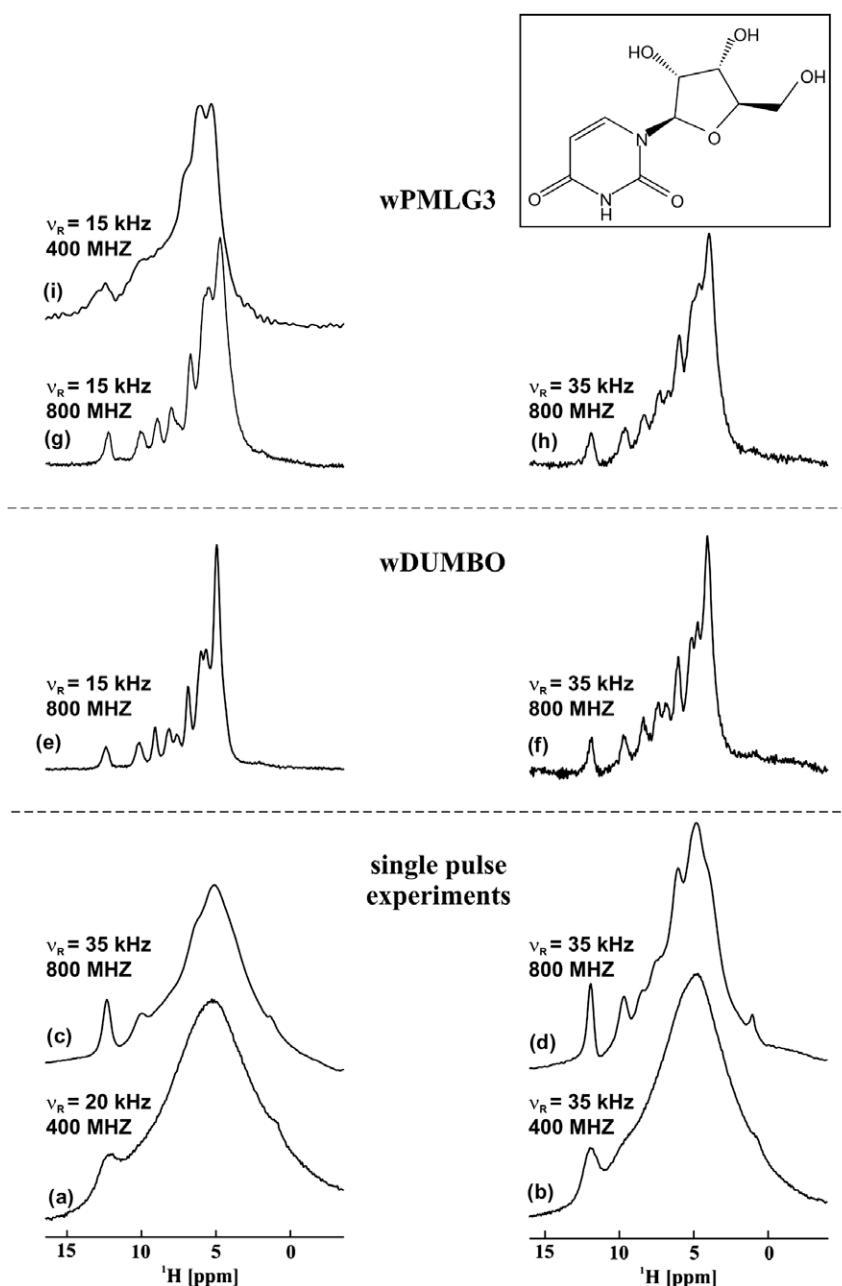

Fig. 4. [1]H uridine spectra recorded employing (a–d) ^{1}H SPE; wDUMBO decoupling using (e) $\nu_1 = 112$ kHz, (f) $\nu_1 = 146$ kHz; wPMLG3 decoupling using (g) $\nu_1 = 112$ kHz, (h) $\nu_1 = 146$ kHz and (i) $\nu_1 = 70$ kHz. Recycle delay: 25 s. The experimental scaling factors were (e) $\lambda_{exp} = 0.61$; (f) $\lambda_{exp} = 0.61$; (g) $\lambda_{exp} = 0.65$; (h) $\lambda_{exp} = 0.73$ and (i) $\lambda_{exp} = 0.69$.

3.2. Investigating windowed ^1H CRAMPS on uridine and GSH tripeptide

In this second part, the robustness of ^1H CRAMPS decoupling techniques, applied to the more complex systems uridine (Fig. 4), a nucleoside, and the GSH (Fig. 5) tripeptide, is evaluated. Here, we are not particularly concerned with the detailed attribution of the different ^1H resonances, which will be reported in a forthcoming paper. Rather, we wish to compare and discuss the different decoupling schemes, and illustrate the high-quality ^1H CRAMPS spectra recorded using cutting edge NMR equipment on these more challenging solids. To better judge the performance of the different windowed ^1H CRAMPS schemes, experiments were performed at different spinning rates and B_0 magnetic fields.

Fast MAS is often required to remove 2nd rank interactions, such as chemical shift anisotropy, which increases at higher B_0 fields. Thus, it is important to have at our disposal ^1H homonuclear decoupling sequences that perform well at high-spinning rates. A series of ^1H spectra recorded at 15–20 (Fig. 4) and 35 kHz (Fig. 5)

MAS rates were acquired on uridine and GSH. The ^1H CRAMPS spectrum of the former (Fig. 4) exhibits a maximum of nine ^1H resonances in the range $\delta = 4$–12 ppm. For GSH (Fig. 5), 10 ^1H resonances are resolved ranging from 2 to 14 ppm. The resonance at $\delta_H \cong 13.3$ ppm and the two overlapped resonances at $\delta_H \cong 8.5$ ppm are attributed, respectively to –COOH and –NH/–NH$_3$ groups. Seven peaks are observed in the 1.8–4.4 ppm region. Six are tentatively attributed to the different –CH and –CH_2 groups and one shoulder at $\delta_H \cong 1.8$ ppm, assigned to the $-SH$ group (Fig. S2). A dedicated assignment study will be addressed elsewhere for uridine and GSH compounds.

3.2.1. Comparing and testing windowed ^1H CRAMPS methods

Again, faster spinning rates leads to better resolved ^1H SPE spectra. Increasing B_0 only, from 9.4 to 18.8 T, in ^1H SPE do not lead to a drastic ^1H spectral resolution improvement for uridine (Fig. 4ac and bd) and GSH (Fig. 5ac and bd). The same behavior is noticed when comparing the ^1H SPE with $v_R = 20$ and 35 kHz spectra of uri-
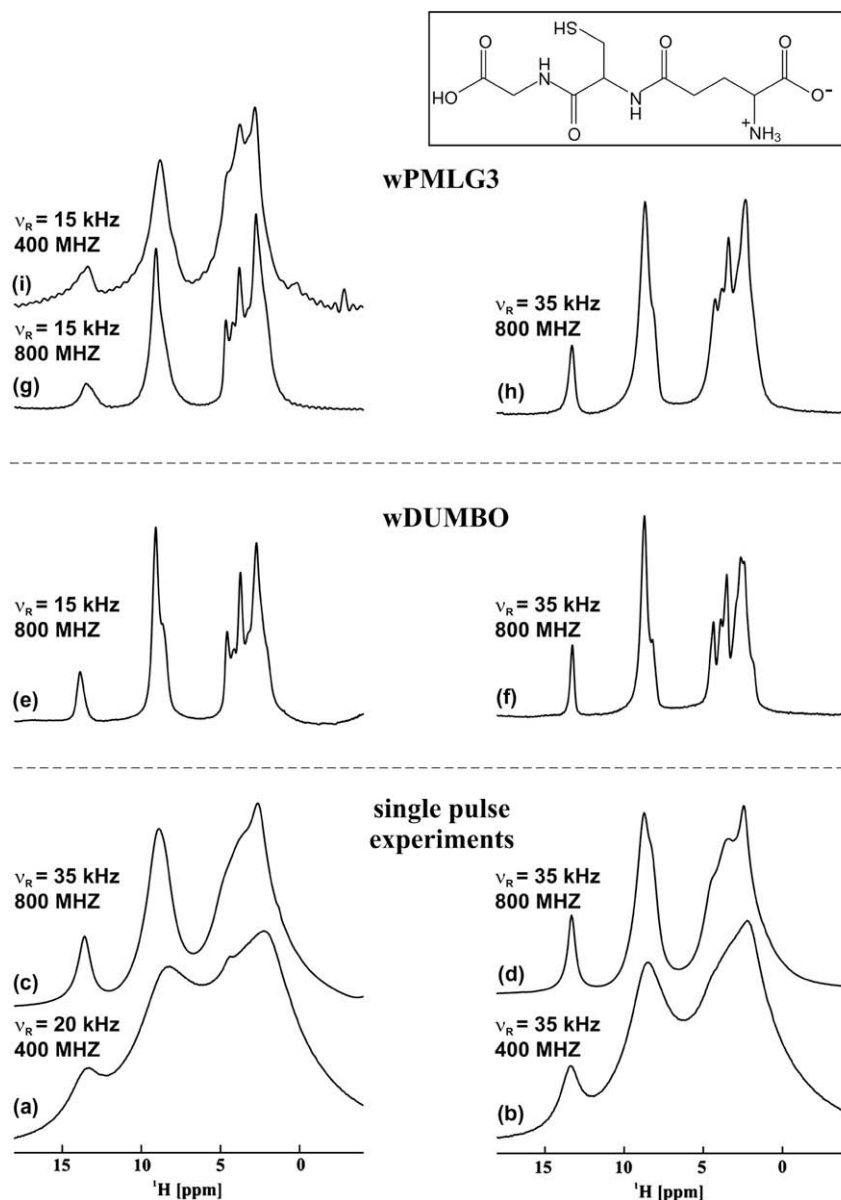

Fig. 5. ^1H GSH spectra recorded employing (a–d) ^1H SPE; wDUMBO decoupling using (e) $v_1 = 112$ kHz, (f) $v_1 = 146$ kHz; wPMLG3 decoupling using (g) $v_1 = 112$ kHz, (h) $v_1 = 146$ kHz and (i) $v_1 = 70$ kHz. Recycle delay: 5 s. The experimental scaling factors were (e) $\lambda_{exp} = 0.57$; (f) $\lambda_{exp} = 0.61$; (g) $\lambda_{exp} = 0.57$ and (h) $\lambda_{exp} = 0.72$.

dine (Fig. 4ab and cd) and GSH (Fig. 5ab and cd). On the other hand, the ^{1}H CRAMPS spectra (Fig. 4e–h and 5e–h for uridine and GSH, respectively) present comparable resolution at 15 (or even lower) and 35 kHz, which is much better than the resolution of the ^{1}H SPE at ν_R = 35 kHz. For example, the ^{1}H wPMLG3 (Fig. 4e) or wDUMBO (Fig. 4g) spectra of uridine recorded at 15 kHz exhibit a resolution similar relative to those recorded at 35 kHz (Fig. 4f and h). Note that although four times more scans have been used to record the ^{1}H CRAMPS uridine spectra at ν_R = 35 kHz than the spectrum at ν_R = 15 kHz, the former still shows a weaker signal-to-ratio due to the need of a smaller sample volume to rotate the sample at ν_R = 35 kHz. Consider now the performance of wDUMBO and wPMLG3 techniques. For uridine, the spectra of the former show slightly better resolution at different spinning rates (compare Fig. 4e with Fig. 4g and Fig. 4f with Fig. 4h). In particular, the uridine peaks at δ_H = 5.5 and 7.5 ppm clearly show this. For GSH at moderate spinning rates both decoupling strategies afford similar spectral resolution (Fig. 5e and g). However, differences in the resolution afforded by the two methods are observed in the 1.8–4.4 ppm region at ν_R = 35 kHz (Fig. 5f and h). Such differences are, mainly, due to the wDUMBO ^{1}H decoupling improvement at high spinning rates (Fig. 5f).

It is clear from Figs 4 and 5 that changing the spinning rate alone does not yield a very considerable resolution enhancement. In addition, ^{1}H CRAMPS decoupling at B_0 = 9.4 T performs the same or worse than ^{1}H SPE (ν_R = 35 kHz) alone at 18.8 T. We must emphasize that employing high-field and ^{1}H CRAMPS decoupling simultaneously is the best solution to obtain highly resolved ^{1}H NMR spectra (Fig. 4e–h and Fig. 5e–h).

4. Conclusion

The influence of the spinning rate, rf decoupling cycle, nutation frequency and B_0 field on the resolution of ^{1}H NMR spectra has been assessed using three different ^{1}H CRAMPS schemes. Although wPMLG3, wDUMBO and wSAM3 have been studied, special attention was given to the former two. It has been shown that windowed ^{1}H CRAMPS techniques, (wPMLG3 and wDUMBO) designed for relatively slow spinning rates, perform very well up to 35 kHz (affording slightly better resolution than that of the 10–15 kHz spectra). The spectral resolution obtained with, wPMLG3 and wDUMBO is better than the resolution yielded by wSAM3 technique, for spinning rates up to 35 kHz. Although the wPMLG3 and wDUMBO ^{1}H spectral resolutions are very similar, sometimes the latter outperforms the former. Such quasi-static derived techniques should perform well at the presently available very-fast spinning speeds (ca. 70 kHz) provided the adequate τ_R/τ_C is chosen. Such MAS rates will need larger rf field strengths, which are not a limitation since the smaller size of the high MAS rate spinners offer the possibility of delivering considerably stronger rf fields. At the maximum spinning rate available to us (ν_R = 35 kHz) best ^{1}H decoupling is reached at $\tau_R/\tau_C \cong 1.5$ using an rf field strength of 150 kHz.

Windowed ^{1}H acquisition schemes have the advantage of affording highly resolved ^{1}H spectra in a single dimension, thus opening the possibility to be used during t_2 evolution in 2D pulse schemes where high-resolution ^{1}H detection may help performing, otherwise, insensitive experiments. Work along this line is in progress.

Appendix A. Supplementary data

Supplementary data associated with this article can be found, in the online version, at doi:10.1016/j.jmr.2008.11.010.

References

[1] R.K. Harris, P. Jackson, L.H. Merwin, B.J. Say, G. Hagele, Perspectives in high-resolution solid-state nuclear magnetic-resonance with emphasis on combined rotation and multiple-pulse spectroscopy, J. Chem. Soc. Faraday Trans. I 84 (1988) 3649–3672.
[2] J.W. Traer, E. Montoneri, A. Samoson, J. Past, T. Tuherm, G.R. Goward, Unraveling the complex hydrogen bonding of a dual-functionality proton conductor using ultrafast magic angle spinning NMR, Chem. Mater. 18 (2006) 4747–4754.
[3] B.C. Gerstein, C. Chow, R.G. Pembleton, R.C. Wilson, Utility of pulse nuclear magnetic-resonance in studying protons in coals, J. Phys. Chem. 81 (1977) 565–570.
[4] P. Mansfield, Symmetrized pulse sequences in high resolution NMR in Solids, J. Phys. Part C Solid State Phys. 4 (1971) 1444–1452.
[5] W.K. Rhim, D.D. Elleman, R.W. Vaughan, Analysis of multiple pulse NMR in solids, J. Chem. Phys. 59 (1973) 3740–3749.
[6] J.S. Waugh, L.M. Huber, U. Haeberle, Approach to high-resolution NMR in solids, Phys. Rev. Lett. 20 (1968) 180–182.
[7] D.G. Cory, A new multiple-pulse cycle for homonuclear dipolar decoupling, J. Magn. Reson. 94 (1991) 526–534.
[8] D.P. Burum, M. Linder, R.R. Ernst, Low-power multipulse line narrowing in solid-state NMR, J. Magn. Reson. 44 (1981) 173–188.
[9] M. Hohwy, P.V. Bower, H.J. Jakobsen, N.C. Nielsen, A high-order and broadband CRAMPS experiment using z-rotational decoupling, Chem. Phys. Lett. 273 (1997) 297–303.
[10] A. Bielecki, A.C. Kolbert, M.H. Levitt, Frequency-switched pulse sequences—homonuclear decoupling and dilute spin NMR in solids, Chem. Phys. Lett. 155 (1989) 341–346.
[11] B.J. vanRossum, H. Forster, H.J.M. deGroot, High-field and high-speed CP-MAS C-13 NMR heteronuclear dipolar-correlation spectroscopy of solids with frequency-switched Lee–Goldburg homonuclear decoupling, J. Magn. Reson. 124 (1997) 516–519.
[12] E. Vinogradov, P.K. Madhu, S. Vega, High-resolution proton solid-state NMR spectroscopy by phase-modulated Lee–Goldburg experiment, Chem. Phys. Lett. 314 (1999) 443–450.
[13] E. Vinogradov, P.K. Madhu, S. Vega, A bimodal Floquet analysis of phase modulated Lee–Goldburg high resolution proton magic angle spinning NMR experiments, Chem. Phys. Lett. 329 (2000) 207–214.
[14] E. Vinogradov, P.K. Madhu, S. Vega, Phase modulated Lee–Goldburg magic angle spinning proton nuclear magnetic resonance experiments in the solid state: a bimodal Floquet theoretical treatment, J. Chem. Phys. 115 (2001) 8983–9000.
[15] A. Lesage, D. Sakellariou, S. Hediger, B. Elena, P. Charmont, S. Steuernagel, L. Emsley, Experimental aspects of proton NMR spectroscopy in solids using phase-modulated homonuclear dipolar decoupling, J. Magn. Reson. 163 (2003) 105–113.
[16] D. Sakellariou, A. Lesage, P. Hodgkinson, L. Emsley, Homonuclear dipolar decoupling in solid-state NMR using continuous phase modulation, Chem. Phys. Lett. 319 (2000) 253–260.
[17] B. Elena, G. de Paepe, L. Emsley, Direct spectral optimisation of proton–proton homonuclear dipolar decoupling in solid-state NMR, Chem. Phys. Lett. 398 (2004) 532–538.
[18] C. Coelho, J. Rocha, P.K. Madhu, L. Mafra, Practical aspects of Lee–Goldburg based CRAMPS techniques for high-resolution 1H NMR spectroscopy in solids: implementation and applications, J. Magn. Reson. 194 (2008) 264–282.
[19] D.P. Burum, W.K. Rhim, Analysis of multiple pulse NMR in solids 3, J. Chem. Phys. 71 (1979) 944–956.
[20] L. Bosman, P.K. Madhu, S. Vega, E. Vinogradov, Improvement of homonuclear dipolar decoupling sequences in solid-state nuclear magnetic resonance utilising radiofrequency imperfections, J. Magn. Reson. 169 (2004) 39–48.
[21] M. Leskes, P.K. Madhu, S. Vega, Proton line narrowing in solid-state nuclear magnetic resonance: new insights from windowed phase-modulated Lee–Goldburg sequence, J. Chem. Phys. 125 (2006).
[22] M.H. Levitt, A.C. Kolbert, A. Bielecki, D.J. Ruben, High-resolution H-1-NMR in solids with frequency-switched multiple-pulse sequences, Solid State Nucl. Magn. Reson. 2 (1993) 151–163.

[23] E. Vinogradov, P.K. Madhu, S. Vega, Proton spectroscopy in solid state nuclear magnetic resonance with windowed phase modulated Lee–Goldburg decoupling sequences, Chem. Phys. Lett. 354 (2002) 193–202.

[24] S. Hafner, H.W. Spiess, Multiple-pulse line narrowing under fast magic-angle spinning, J. Magn. Reson. Ser. A 121 (1996) 160–166.

[25] P.K. Madhu, X. Zhao, M.H. Levitt, High-resolution H-1 NMR in the solid state using symmetry-based pulse sequences, Chem. Phys. Lett. 346 (2001) 142–148.

[26] S. Paul, R.S. Thakur, P.K. Madhu, H-1 homonuclear dipolar decoupling at high magic-angle spinning frequencies with rotor-synchronised symmetry, Chem. Phys. Lett. 456 (2008) 253–256.

[27] J.P. Amoureux, B. Hu, J. Trebosc, Enhanced resolution in proton solid-state NMR with very-fast MAS experiments, J. Magn. Reson. 193 (2008) 305–307.

[28] J.-P. Amoureux, B. Hu, J. Trébosc, Q. Wang, O. Lafon, F. Deng, Homonuclear dipolar decoupling schemes for fast MAS, Solid State Nucl. Magn. Reson., in press. Available online 18 November 2008.

[29] L. Mafra, J.R.B. Gomes, J. Trebosc, J. Rocha, J.-P. Amoureux, 2D 1H-1H double-quantum CRAMPS NMR at very-fast MAS: a resolution enhancement method to probe 1H–1H proximities in solids, J. Magn. Reson. 196 (2009) 88–91.

[30] M. Lee, W.I. Goldburg, Nuclear-magnetic-resonance line narrowing by a rotating rf field, Phys. Rev. 140 (1965) 1261.

[31] M. Leskes, P.K. Madhu, S. Vega, A broad-banded *z*-rotation windowed phase-modulated Lee–Goldburg pulse sequence for H-1 spectroscopy in solid-state NMR, Chem. Phys. Lett. 447 (2007) 370–374.

[32] C. Filip, S. Hafner, Analysis of multiple-pulse techniques under fast MAS conditions, J. Magn. Reson. 147 (2000) 250–260.

[33] V.E. Zorin, M. Ernst, S.P. Brown, P. Hodgkinson, Insights into homonuclear decoupling from efficient numerical simulation: techniques and examples, J. Magn. Reson. 192 (2008) 183–196.

[34] S. Hafner, H.W. Spiess, Multiple-pulse assisted line-narrowing by fast magic-angle spinning, Solid State Nucl. Magn. Reson. 8 (1997) 17–24.